Inorganic Chemistry Communications 170 (2024) 113332

Contents lists available at ScienceDirect

Inorganic Chemistry Communications

journal homepage: www.elsevier.com/locate/inoche

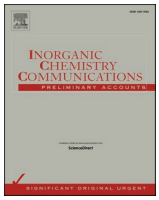

Unveiling the potential of PVA-Er_2O_3 films for superior optical, electrical, mechanical, and thermal applications

T.S. Soliman [a,b,*], A. Khalid [c], M. Khalid Hossain [d], Sherief A. Al kiey [e,f]

[a] Institute of Natural Sciences and Mathematics, Ural Federal University, Ekaterinburg 620000, Russia
[b] Physics Department, Faculty of Science, Benha University, Benha 13518, Egypt
[c] Department of Basic Engineering Sciences, Faculty of Engineering at Shoubra, Benha University, Cairo, Egypt
[d] Institute of Electronics, Atomic Energy Research Establishment, Bangladesh Atomic Energy Commission, Dhaka 1349, Bangladesh
[e] Electrochemistry and Corrosion Lab, Physical Chemistry Department, National Research Centre, Dokki, Cairo 12622, Egypt
[f] Material Engineering Lab., Central Network Laboratories, National Research Centre, Dokki, Cairo 12622, Egypt

ARTICLE INFO

Keywords:
PVA
Er_2O_3
Mechanical properties
UV–visible spectroscopy
Cole-Cole plots
Argand plots

ABSTRACT

This study explores the enhancement of polyvinyl alcohol (PVA) films by incorporating erbium oxide (Er_2O_3) nanoparticles using the casting solution method. We investigated the structural, optical, electrical, dielectric, and mechanical properties of PVA-Er_2O_3 nanocomposite films with varying Er_2O_3 concentrations (2.5, 5, 7.5, and 10 wt%). Structural analyses confirmed successful nanoparticle integration. Optical measurements revealed reduced transparency and bandgap, alongside increased refractive index. Electrical conductivity showed significant improvement with Er_2O_3 inclusion. Dielectric properties demonstrated enhanced performance, with frequency-dependent studies and Argand plot analysis providing insights into charge transport and relaxation mechanisms. Mechanical testing indicated increased tensile strength and Young's modulus, with the 10 wt% nanocomposite showing comparable performance to pure PVA. These findings highlight the potential of PVA-Er_2O_3 films for advanced applications in electronics, sensors, and energy storage systems.

1. Introduction

New generations of photonic and electronic devices are dependent on smart, flexible, and cheap materials, which provide fascinating characteristics. Polymer nanocomposite materials provide flexibility and ease of handling, but researchers are still working on enhancing their characteristics. Recent years have seen a significant increase in interest in polyvinyl alcohol (PVA) as a versatile and promising material for a range of applications because of its superior film-forming capabilities, biodegradability, and compatibility with a broad spectrum of additives [1–4]. PVA can be tuned to enhance its properties by incorporating nanoparticles into its matrix. Various metal oxides have been used as a dopant material in the PVA matrix, like SiO_2 [5], CuO [6], ZnO [7], TiO_2 [8,9], NiO [10], Co_2O_3–SiC [11], etc. Recently, researchers have used rare earth oxides as a dopant material in polymer matrices to enhance their electrical and optical parameters, besides their wide use in different fields like sensors, display, and laser applications [12]. Y_2O_3 was used as a filler material in the PVA matrix and showed improvements in the optical and electrical parameters and the optioned polymer films were recommended for shielding applications [13]. Composite combining CeO_2 and GdO_2 doped with Er_2O_3 are reinforced in siloxane polymer matrix to enhance their photoluminescence properties for photonic applications [14]. The impact of Y_2O_3 nanosheets on the electrical and optical properties of a blend matrix combining polyethylene glycol and polyvinyl chloride has been investigated [15]. The optical and electrical parameters showed an enhancement with increasing the Y_2O_3 content in the blend matrix. $ErCl_3$ doped into the PVA matrix with different amounts showed an increment in the refractive index and a decline in the bandgap energy of the polymer composite film [12]. La_2O_3 showed improvements in the linear and nonlinear optical parameters of the polyvinyl chloride matrix [16]. Er^{+3} and Dy^{+3} nanoparticles were added to the PVA matrix to enhance the shielding applications [17]. Owing to their unique optical properties, Er_2O_3 was used as a filler material in various polymer matrices, for instance in polycaprolactone-polyethylene glycol blend [18], polymethyl methacrylate [19], carboxymethyl cellulose/polyvinyl alcohol blend [20], polyvinyl chloride/polyvinylpyrrolidone blend [21], poly(ethylene oxide)-poly(vinyl chloride) blend [22], and poly(vinylidene fluoride)

* Corresponding author.
E-mail address: tarek.attia@fsc.bu.edu.eg (T.S. Soliman).

https://doi.org/10.1016/j.inoche.2024.113332
Received 18 May 2024; Received in revised form 17 September 2024; Accepted 14 October 2024
Available online 18 October 2024

[23].

The high atomic number of erbium, combined with its thermal stability and distinctive electronic structure, imparts remarkable features to the PVA-Er_2O_3 composite [18]. This synthesis results in a composite material, referred to as PVA-Er_2O_3 film, exhibiting unique characteristics that make it an attractive candidate for applications in both conductivity and dielectric devices. As a result, the PVA- Er_2O_3 film becomes a subject of interest for researchers and engineers seeking advanced materials with enhanced conductivity and dielectric properties. This introduction aims to provide an overview of the motivation behind the synthesis of PVA-Er_2O_3 films, highlighting the importance of these composites in emerging technologies related to electrical conductivity and dielectric applications. The motivation behind this research lies in the increasing demand for materials that can address the evolving needs of electronic devices, sensors, and energy storage systems. PVA- Er_2O_3 films present an opportunity to bridge the gap between traditional polymer films and high-performance materials, offering a unique blend of flexibility, stability, and enhanced electrical functionalities. In this comprehensive study, we delve into the intricate details of the synthesis process, elucidating the methodologies employed to ensure a homogenous distribution of Er_2O_3 nanoparticles within the PVA matrix.

In the present work Er_2O_3 was reinforced with different ratios in the PVA matrix to produce new polymer materials for superior optical, electrical, mechanical, and thermal applications. By means of an X-ray diffractometer and Raman spectroscopy, the impact of Er_2O_3 NPs on the structure of the PVA matrix was investigated. The UV–visible spectrophotometer and impedance spectroscopy were used to investigate the optical and electrical properties. Besides the mechanical investigation of the polymer film in terms of the stress–strain curve.

2. Experimental

2.1. Materials and reagents

Er_2O_3 NPs (purity 99.95 %) and polyvinyl alcohol crystals (PVA, molecular weight (M_η) = 1×10^6) were purchased from QualiChem's company, India. Distilled water (DW) was used as a solvent for PVA crystals.

2.2. PVA-Er_2O_3 (PEr) nanocomposite films preparations

PVA crystals with an appropriate amount (5 g) were dissolved in DW (100 ml) in an oven at 70 °C for 2 h and then stirred with a magnetic stirrer at room temperature for 4 h. Er_2O_3 NPs were added to the PVA solution with various weights to obtain 5 nanocomposites solutions, as shown in Table 1. The probe ultrasonic was used to distribute Er_2O_3 NPs in the PVA solution. All prepared solutions were poured directly into glass plates after the sonication process and left in a warm chamber to dry. Then, after several days, the polymer films were removed from the plates and utilized for further investigations. The schematic graph of the experimental work, the color gradient of the obtained polymer films, and the interaction mechanism between the polymer matrix and Er_2O_3 nanoparticles are shown in Scheme 1. The composition of the films, thickness, and their labels are illustrated in Table 1. The thickness of the film was measured using a digital micrometer.

Table 1
Composition and thicknesses of the PEr films.

Film label	PVA weight in gm	Er_2O_3, weight in gm	Thickness, μm
PEr0	1	0	120
PEr1	1	0.025	100
PEr2	1	0.050	100
PEr3	1	0.075	100
PEr4	1	0.10	120

2.3. Characterization techniques

The diffraction pattern of the Er_2O_3 NPs and PEr films were obtained using Brucker D8 XRD, (with X-ray wavelength = 1.5418 Å). A high-resolution Raman microscope Alpha 300 AR (WITec-GmbH, Germany) equipped with a 35 mW He-Ne laser was used to perform the Raman spectra of the Er_2O_3 NPs and PEr films. The optical investigations were performed with the ultraviolet–visible spectrophotometer (model-cary5000) in the range 200–1000 nm. The thermal characteristics of as-prepared nanocomposites were evaluated using (Themsys one plus, SETARAM, France) from room temperature to 600 °C in N_2 atmosphere. The samples under investigation were cut utilizing a dog-bone-shaped die on a flat aluminum sheet with the objective of performing the mechanical tensile evaluations employing a Lloyd LRX5 K (Lloyd Instruments Ltd, United Kingdom) at a crosshead speed of 2 mm/min. Every sample was subjected to three separate identifications before an average was calculated. For the CMC/PAM-0.16 wt% NPs sample, broadband dielectric spectroscopy was used, with an operating voltage of 1 V and a frequency range of 0.1 Hz to 20 MHz, to test the dielectric at 30 °C and various temperatures.

3. Results and discussion

3.1. Structural characterization

3.1.1. XRD analysis

The XRD pattern of Er_2O_3 and PEr nanocomposite films are illustrated in Fig. 1. Firstly, the Er_2O_3 spectrum, Fig. 1a, shows various crystalline diffraction peaks at 20.76°, 29.48°, 34.12°, 49°, and 58.18° which are linked to the (211), (222), (400), (440), and (622) diffraction plans of the cubic phase of Er_2O_3 according to the JCPDS # 01–077-0459 [24].

The Er_2O_3 pattern was fitted using the Origin-software, which can estimate the full width at half maximum (β) of the most intense peak at 29.48° and investigate the average crystallite size ($D_{(222)}$) of Er_2O_3 using the Sherrer's equation as follows [25]:

$$D_{(222)} = \frac{0.9\lambda}{\beta\cos(\theta)} \quad (1)$$

where λ is the X-ray wavelength (0.15418 nm) and θ is the Bragg's diffraction angle. The $D_{(222)}$ value was calculated for the most intense peak at 29.48°, and it was about 39.7 nm. The PEr nanocomposite film diffraction patterns with various Er_2O_3 contents are displayed in Fig. 1b. The main peak of the PVA, which related to the (101) diffraction plane was observed at 19.62°. This peak was shifted towards a higher angle at 19.76°, 20.80°, 20.90°, and 19.76° for PEr1, PEr2, PEr3, and PEr4, respectively, with the inclusion of Er_2O_3 NPs. The same was observed to the (222) plane for the Er_2O_3 NPs, as the peak at 29.48° was shifted to a higher angle at 29.55°, 29.51°, 29.66°, and 29.48° for PEr1, PEr2, PEr3, and PEr4, respectively, as seen in the inset of Fig. 1b. The deviation of the diffraction angle to the higher angles is associated with the decrease of the *d*-spacing between planes and the growth of the crystallite size in the matrix [26]. Furthermore, this deviation is confirmation of a complexation between Er_2O_3 NPs and PVA's molecules [27]. The *D* values for Er_2O_3 in the PVA matrix were calculated and found to be 32, 41, 35, and 37 nm. This fluctuation in particle sizes is related to the clusters formed due to increasing the Er_2O_3 contents in the PVA matrix. Increasing the Er_2O_3 NPS contents causes a decrease in the distance between the particles and increases the density in the polymer matrix. This is confirmed using the optical microscope technique, as shown in Fig. 2.

3.1.2. Optical microscope analysis

Using an optical microscope to study surface morphology is an effective and straightforward method, that has been utilized in various

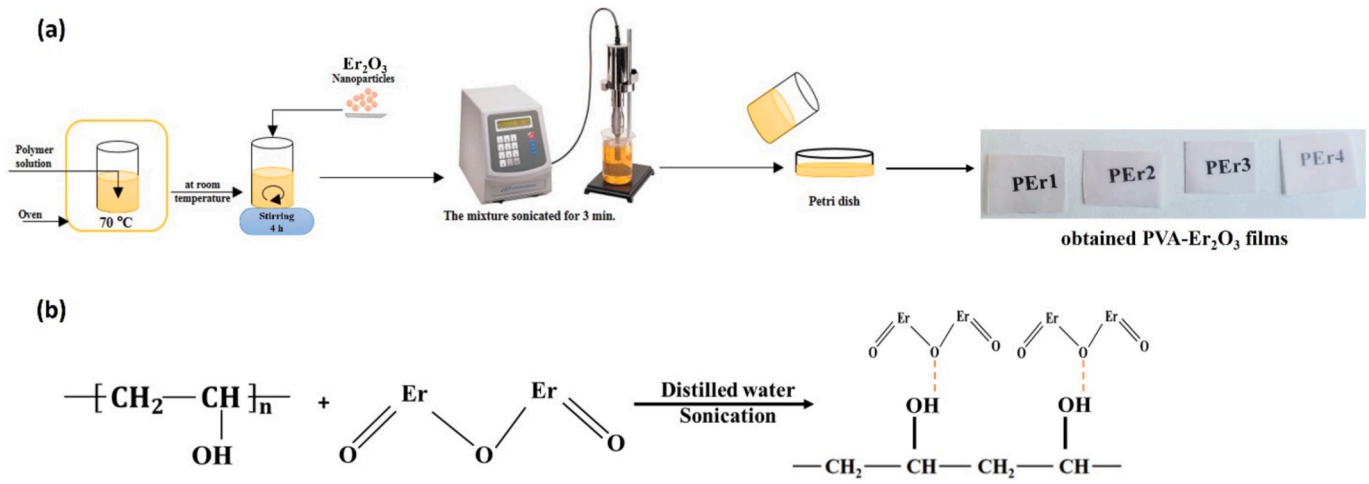

Scheme 1. (a) The PVA-Er_2O_3 film preparation steps and their color gradient after preparation, and (b) the interaction mechanism between PVA molecules and Er_2O_3 nanoparticles.

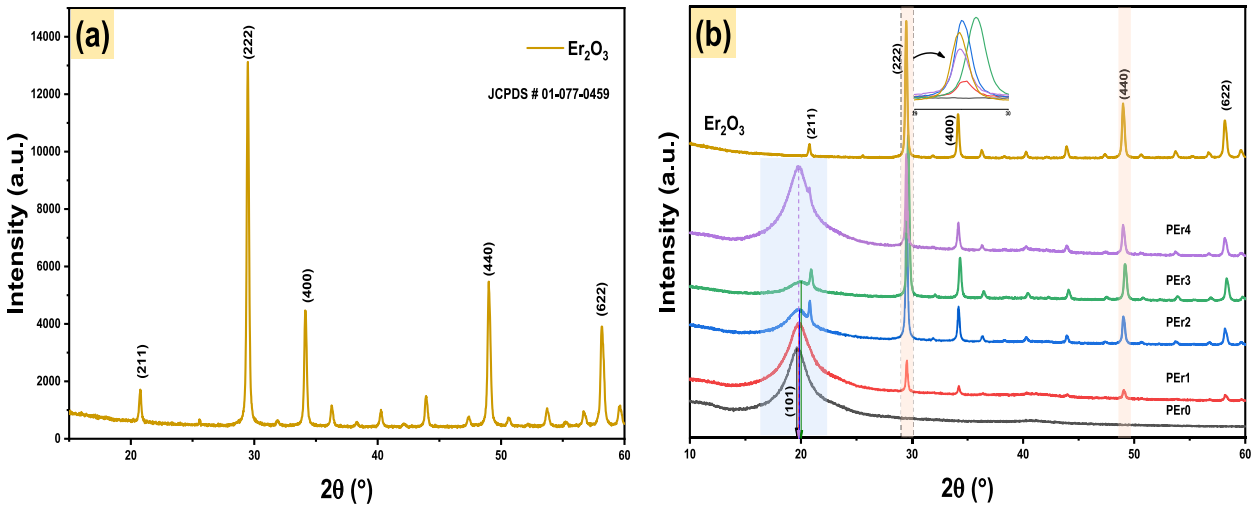

Fig. 1. XRD pattern of (a) Er_2O_3 nanoparticles and (b) PEr nanocomposite films.

investigations [28–34]. Fig. 2 displays the optical microscope images using polarized and unpolarized lenses under magnification 10x for PEr films. Obviously, in Fig. 2a, at a lower content of Er_2O_3 (2.5 %), the black dots, which represent Er_2O_3 NPs, are distributed uniformly in the background (PVA matrix), besides a few big particles formed because of the agglomerations. The same pattern was taken under a polarized lens, as shown in Fig. 2a'. The bright dots represent the metals under the polarized microscope, while the dark background represents the polymer matrix, consistent with the literature [35–39]. As the Er_2O_3 concentration increases in the matrix, the number of dark dots increases (Fig. 2b-d), and the count of big particles also increases, and the distances between the particles become narrower. On the other side for the polarized photos (Fig. 2b'-d'), the bright particles increase in count, and their size increases, indicating obvious aggregation [35]. This result was confirmed by investigating the crystallite size distribution using the *ImageJ* software and drawing the histogram as shown in Fig. 3. The histogram of the PEr1 sample demonstrates a particle size with a minimum diameter of ~ 0.8 μm and a maximum of ~ 18 μm, while the other samples show a maximum diameter of ~ 21, 22, and 26 μm for the PEr2, PEr3, and PEr4 samples, respectively, and the minimum diameter is approximately the same as for the PEr1 sample. Clearly, the count of big particles increases with increasing contents of Er_2O_3, besides the presence of tiny particles with lower counts.

3.1.3. *Raman analysis*

The Raman spectra of Er_2O_3 NPs and PEr nanocomposite films are illustrated in Fig. 4. The Er_2O_3 spectrum, Fig. 1a, shows vibration mode peaks at 193, 233, 326, 381,429, 480, 662, 1263, and 1355 cm^{-1}, respectively which are linked to Er-O bond of the Er_2O_3 [40,41]. The PEr nanocomposite film Raman spectra with various Er_2O_3 contents are displayed in Fig. 4b. The Raman spectra of PEr0 film exhibits 3 Raman active modes occurring at 860, 919, and 1439 cm^{-1} [42]. The composite films display a growth in the number of Raman bands and an enhancement in their intensity. After the incorporation of nano Er_2O_3 to the polymer matrix, bands corresponding to nano Er_2O_3 grow at 381, 662, and 1263 cm^{-1}, Furthermore to the PVA peaks appearance. As the concentration of Er_2O_3 nanoparticles increases, the intensity of the peaks increases, and there is a slight shift in the PVA peaks to a higher wavenumber, as shown in Fig. 4b. This result confirms the crystallinity growth of the host matrix due to the intermolecular interaction of PVA molecules with Er_2O_3 nanoparticles [43].

3.1.4. *Thermal characteristics*

The characteristic features of thermal properties of the pure PVA film and the Er_2O_3 nanocomposites were studied with a TGA analyzer, depicted in Fig. 5. According to thermogravimetric analysis (TGA), the pure PVA film exhibits a constant weight loss that occurs in three stages

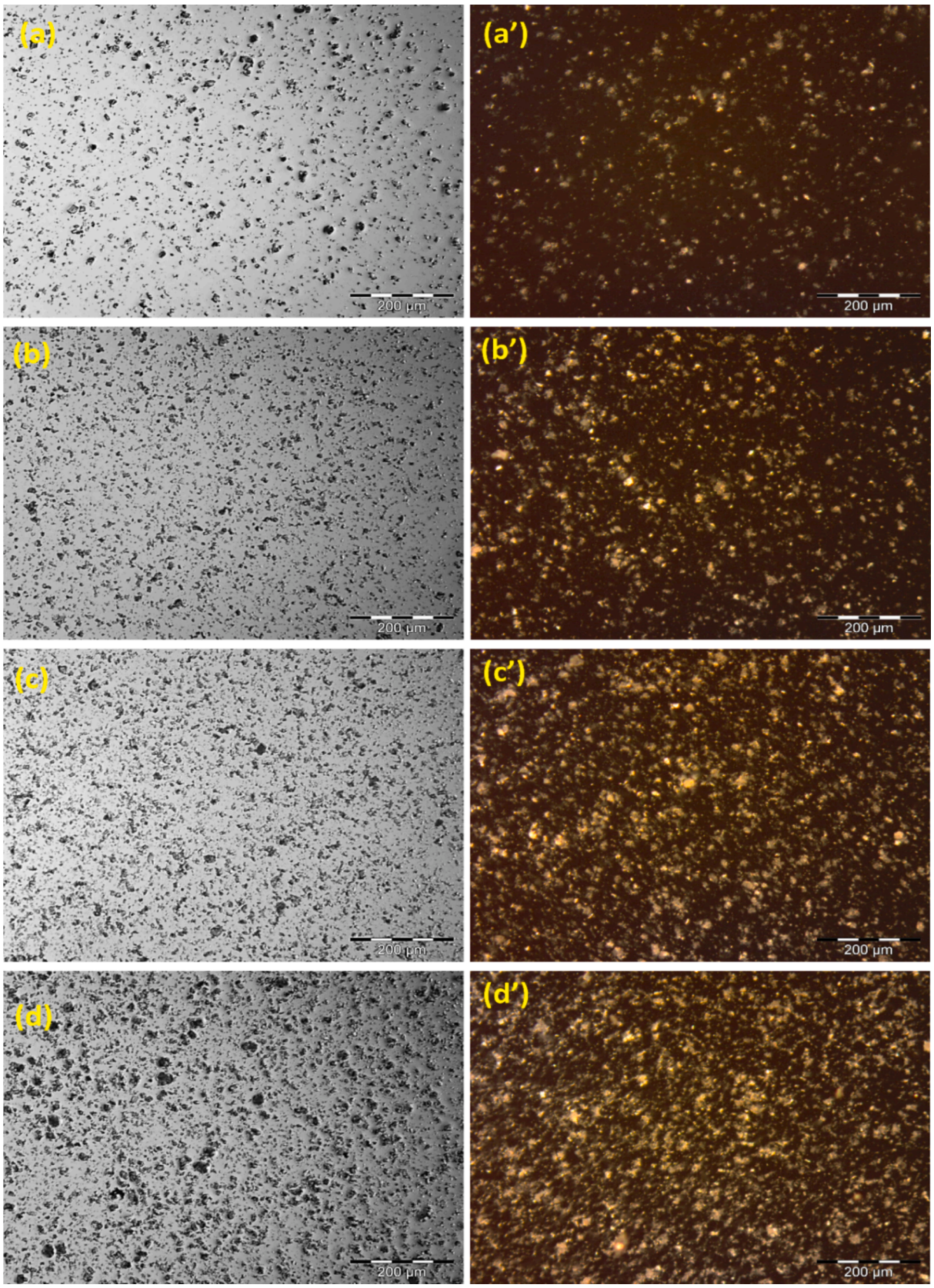

Fig. 2. Optical microscope images for; (a & a') PEr1, (b & b') PEr2, (c & c') PEr3, and (d & d') PEr4 films. (a, b, c, & d) unpolarized lens and (a', b', c', & d') polarized lens.

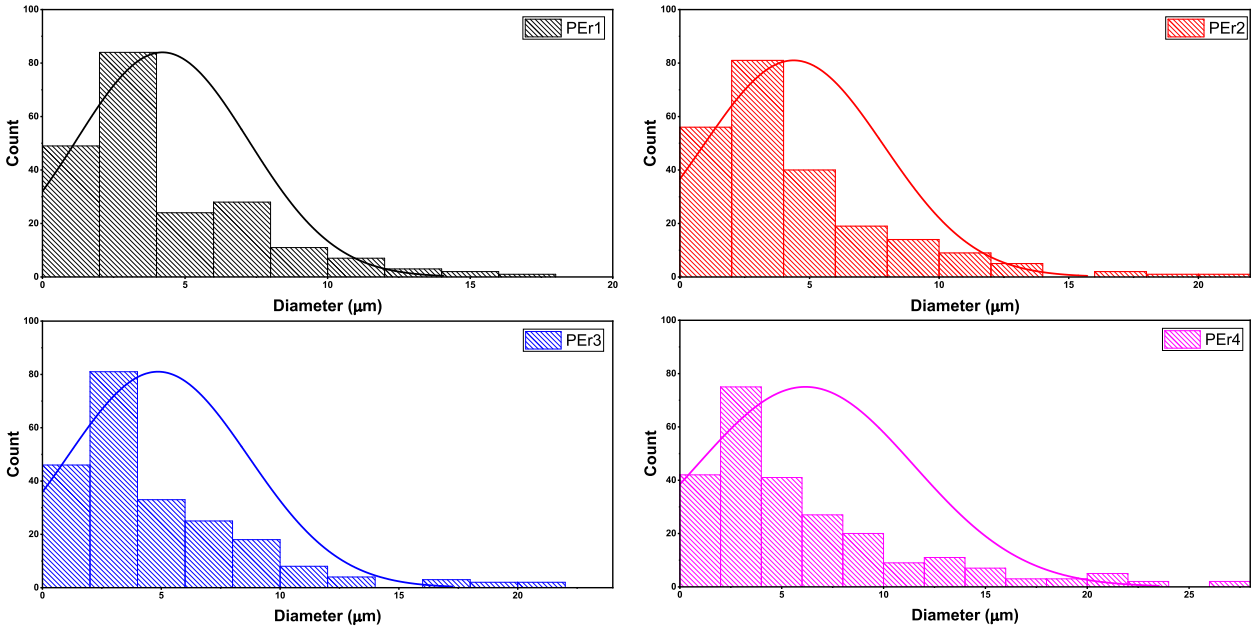

Fig. 3. Histogram of the OM images for PEr nanocomposite films.

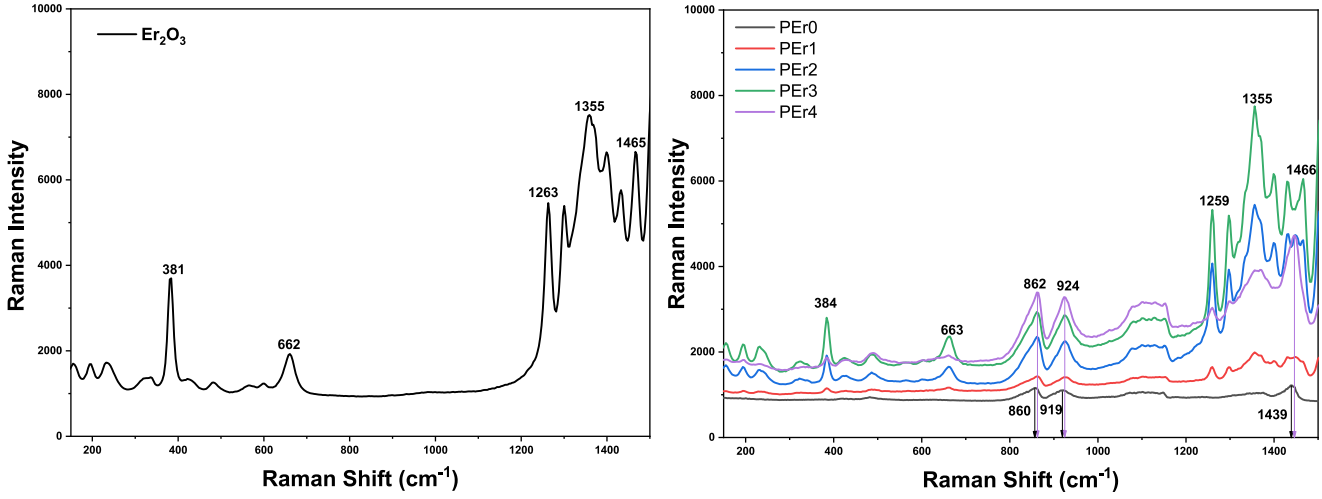

Fig. 4. Raman spectra of; (a) Er_2O_3 NPs and (b) PEr nanocomposite films.

commencing throughout the initial stage of heating, with water evaporation occurring mostly between 60 and 150 °C accounting for the majority of this loss [44]. At temperatures ranging from 230 to 350 °C, the second stage is implemented, the pure sample starts to decompose. The final stage involves breaking down the polymeric structure, which begins around 395 °C and produces carbon and hydrocarbons as byproducts.

It was observed that incorporating Er_2O_3 nanoparticles to the matrix caused the filled samples to be more thermally stable through a decrease in weight loss in TGA scans of PVA- Er_2O_3 nanocomposite samples. Additionally, it displays the total residues of the PVA-Er_2O_3 nanocomposite samples and the pure PVA film samples when heated to 600 °C. These findings demonstrated enhanced thermal stability, which may indicate robust cross-linking between the Er_2O_3 nanofiller and polymeric molecules due to reduced blend chain flexibility and softening [45]. One possible explanation for this improvement is because the Er_2O_3 nanoparticles is evenly distributed throughout the mixture, which effectively stops the breakdown of the polymeric structure [46]. The exceptional thermal stability of the current samples suggests they may find utility as base electrolyte materials in lithium-ion batteries, a technology that relies heavily on such properties.

3.2. *Optical features*

The ultraviolet–visible spectra recorded in terms of absorbance, A, and transmission, T%, as displayed in Fig. 6. Obviously, the PVA absorbance increases with the addition of Er_2O_3 NPs. Besides, the absorption edge extension with the x-axis for the PEr0 sample at 244 nm was shifted to higher wavelengths at 261, 275, 283, and 298 nm for PEr1, PEr2, PEr3, and PEr4 samples, respectively, as clearly seen in Fig. 6a. This result testified to the change in the electronic transition for the PVA and the bandgap changed.

The absorption band observed at 520 nm, for PEr4 sample, is related to one of the multiple absorption bands of Er_2O_3NPs, as mentioned elsewhere [24]. Fig. 6b shows the impact of Er_2O_3 NPs on the film transparency, which decreases from 91 % for the PEr0 sample to 63, 41, 21, and 8 % for PEr1, PEr2, PEr3, and PEr4 samples, respectively. Such a material with low UV transmission can be used in shielding fields. The

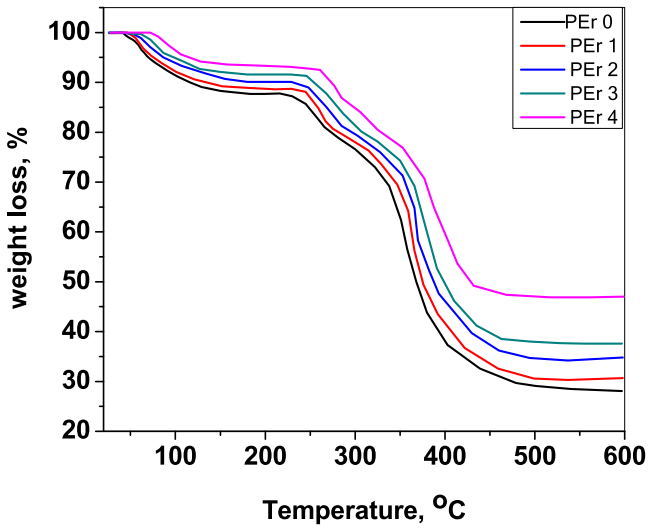

Fig. 5. Thermal gravimetric analysis of PEr nanocomposite films.

investigation of the optical bandgap (E_g) for direct and indirect transitions was done with the help of Tauc's model, which estimates the relation depending on the absorption coefficient (α, cm^{-1}) and the incident photon energy (hυ, eV) of the polymer films as follows [47–49]:

$$(\alpha h\upsilon)^2 = constant(h\upsilon - E_g^{direct}) \quad (2)$$

$$(\alpha h\upsilon)^{1/2} = constant(h\upsilon - E_g^{indirect}) \quad (3)$$

Fig. 7 shows the extraction of bandgap values from straight lines extrapolation with x-axis, at hυ = 0, of the relation between $(\alpha h\upsilon)^2$ and $(\alpha h\upsilon)^{1/2}$ against (hυ). The extracted E_g values are illustrated in Table 2.

As the Er_2O_3 NPs content increased in the PVA matrix, the bandgap value, direct or indirect, declined. The E_g^{direct} declined from 5.51 eV (for PEr0) to 5.33 eV (PEr1), 5.09 eV (PEr2), 4.87 eV (PEr3), and 4.67 eV (PEr4). The $E_g^{indirect}$ declined from 4.73 eV (for PEr0) to 4.21 eV (PEr1), 3.71 eV (PEr2), 3.53 eV (PEr3), and 3.45 eV (PEr4). This decline in the bandgap value is related to the complex transfer charge exhibited as a result of the defects produced in the matrix, which causes the formation of new levels between the valance and conduction bands [50]. The Er^{+3} ions cause a change in the structure of the polymer matrix as the weak Er-O bonds form between Er_2O_3 NPs and the PVA molecules and cause a decrease in the bandgap energy of the new matrix [51]. The band tail width (E_U) of the films was investigated to assure the raising of the disorder in the polymer films with the inclusion of Er_2O_3 NPs, which was done through Urbach relation as follows [52]:

Table 2
Optical parameters for per nanocomposite films.

Sample ID	$E_g^{direct}(eV)$	$E_g^{indirect}(eV)$	E_U (eV)	n	M(E_g)	M(*n*)
PEr0	5.51	4.73	0.45	1.928	0.52	0.54
PEr1	5.33	4.21	1.10	1.952	0.51	0.53
PEr2	5.09	3.71	1.73	1.987	0.50	0.51
PEr3	4.87	3.53	1.85	2.019	0.49	0.50
PEr4	4.67	3.45	1.46	2.051	0.48	0.48

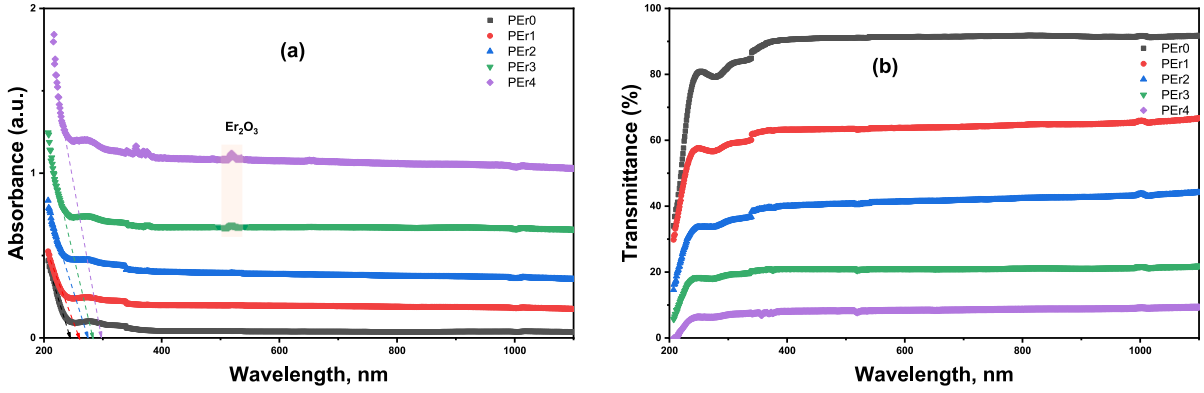

Fig. 6. Ultraviolet–visible spectra (a) A and (b) T% for PEr nanocomposite films.

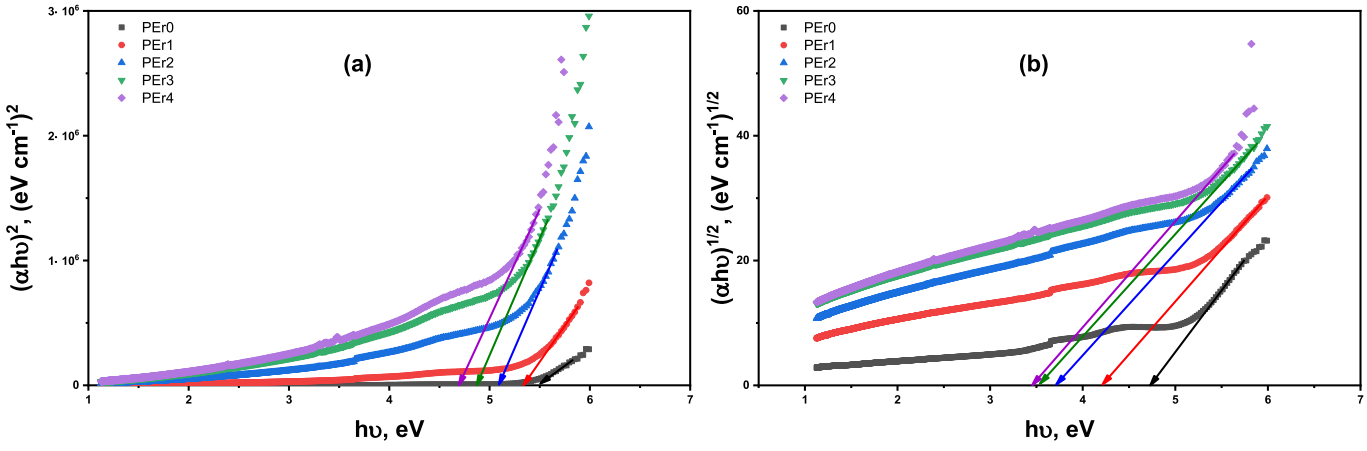

Fig. 7. (a) $(\alpha h\upsilon)^2$ and (b) $(\alpha h\upsilon)^{1/2}$ against (hυ) for PEr nanocomposite films.

$$Ln(\alpha) = Ln(\alpha_0) + \frac{h\upsilon}{E_U} \quad (4)$$

The obtained E_U values from drawing the relation between Ln(α) and hυ, as seen in Fig. 8, are represented in Table 2. As the Er_2O_3 NPs content increases in the PVA matrix, the E_U value increases as well. This confirms the increase in polymer disordering and decreases the forbidden zone.

The nature of the impact of the incident light on the material is obtained from the relation between the index of material refraction (n) and E_g, which is proposed by the Lorentze-Lorentze equation as follows [53]:

$$1 - \frac{n^2 - 1}{n^2 + 2} = \left(\frac{E_g}{20}\right)^{1/2} \quad (5)$$

Table 2 displays the computed *n* values. Obviously, the *n* value increases with increasing the additives in the polymer matrix, which could be linked with the growth of density and polarizability of the polymer film. Increasing Er^{+3} ions in the polymer matrix causes an increase in the film's polarizability and its coordination number, and hence the refractive index increases as well [51,54]. Also, the metallic nature of the prepared polymer films can be evaluated in terms of molar refractive index (R_m) and molar volume (V_m) as follows [53]:

$$M = 1 - \frac{R_m}{V_m} = 1 - \frac{n^2 - 1}{n^2 + 2} \quad (6)$$

The metallization criterion (M) values were computed and displayed in Table 2. The M value was observed to decrease with increasing the Er_2O_3 content in the polymer matrix. This decline in the M value is an indication of the increase in the metallic nature of the polymer films [51,53,54]. The R_m/V_m value increases approximately from 0.47 (PEr0) to 0.48 (PEr1), 0.49 (PEr2), 0.50 (PEr3), and 0.51 (PEr4). The larger the R_m/V_m value, the narrower the forbidden zone and the more metallic the obtained material [53].

3.3. Dielectric properties

The frequency variation that is affected by the dielectric constant (ε′) and dielectric loss (ε″) can be calculated using the following equations [55–57]:

$$\varepsilon' = Ct/(\varepsilon_\circ . A) \quad (7)$$

$$\varepsilon'' = \sigma'/(\omega.\varepsilon_\circ) \quad (8)$$

In this equation, C stands for the observed capacitance, $\varepsilon_\circ$ for the free-space permittivity, t for the sample thickness, A for the electrodes' cross-sectional area, ω for the angular frequency, and σ′ for the actual portion of electrical conductivity.

The parameter ε′ provides insights into the material's ability to store electrical energy when exposed to an electric field. In our study, the enhancement in ε′ due to the incorporation of Er_2O_3 nanoparticles indicates improved polarization behavior and charge storage capacity. This is particularly important for applications in capacitors, energy storage systems, and microelectronics, where materials with higher dielectric constants are desirable for efficient energy storage and signal processing. Studying dielectric loss ε′′ reveals the material's energy dissipation during the polarization process, which is critical for determining the efficiency and stability of the material under alternating current (AC) conditions. Low dielectric loss suggests that the material can efficiently store energy with minimal loss, making it suitable for applications in sensors, antennas, and other dielectric devices [58].

At room temperature, the film samples' ε′ and ε″ across a range of frequencies were systematically studied as displayed in Fig. 9 a and b, respectively. A significant enhancement in the dielectric constant was observed compared to pristine PVA films, indicating the influence of Er_2O_3 nanoparticles on the material's polarization behavior. It is believed that the structure of polymers will improve the value of ε′ as well as the permittivity values of the Er_2O_3 nanoparticles and the host PVA film as a result of interactions and intermolecular hydrogen bonding within the significant Maxwell-Wagner-Silars (M−W−S) process of interfacial polarization, which exists at the lowest frequency value [59,60]. This augmentation can be attributed to the polar nature of Er_2O_3 nanoparticles, contributing to increased polarization and improved charge storage capacity within the composite [61]. The value of ε′ diminishes while the frequency increases because dipoles are unable to align with the path of an external field at exceptionally high frequencies [62,63]. This is because the dipoles are oriented with the presence of the field. Therefore, at the high-frequency section, the value of ε′ stabilizes and then decreases.

The dielectric permittivity values of the occupied samples are improved due to the electrostatic interaction between the dipole groups of the PVA film and the Er_2O_3 nanoparticles. This interaction facilitates the dipole arrangement of polar PVA, as well as the higher ε′ value of Er_2O_3 nanoparticles, which could be responsible for this improvement in ε′ values [64]. Nanocomposites exhibit an enhanced charge carrier efficiency than pure PVA films, leading to an increase in ε″ values as the

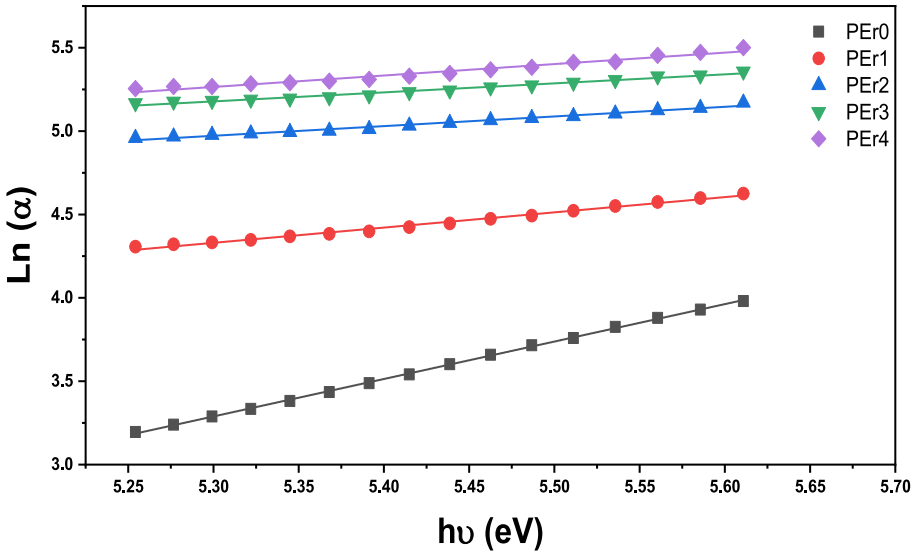

Fig. 8. Ln(α) vs. (hυ) for PEr nanocomposite films.

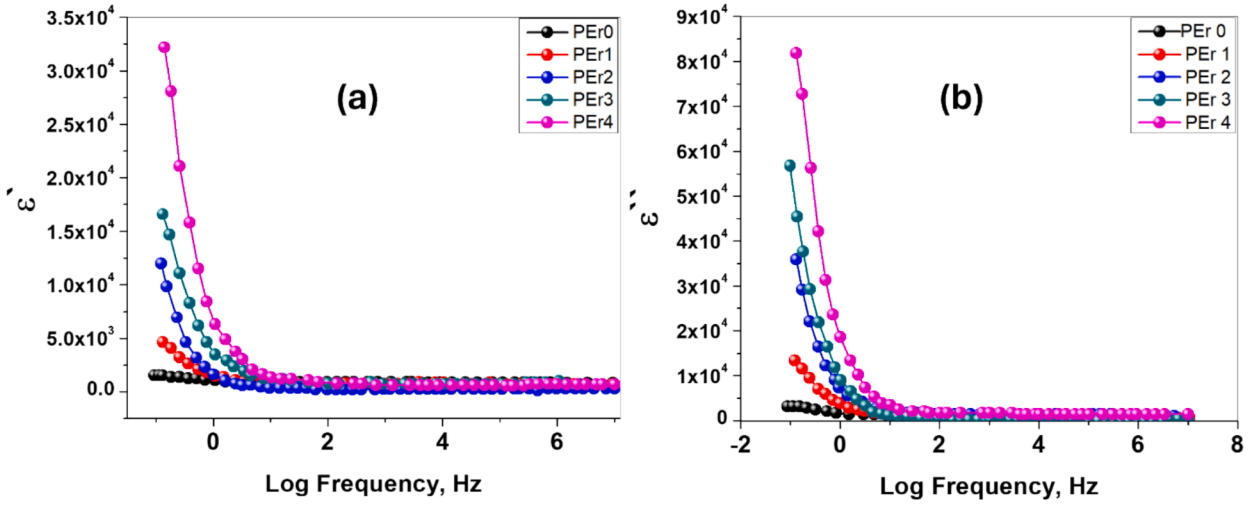

Fig. 9. Variation of (a) ε′ and (b) ε″ plots vs. frequency of PEr nanocomposite films.

concentrations of Er_2O_3 nanoparticles rise [65]. A decrease in the value at higher frequencies is caused by an increase in charge mobility inside the PVA film, and it was shown that the lowest frequency occurs when the highest value of ε″ occurred. As a result of charges building up, the polarization value drops. At higher frequencies, the linear difference between ε′ and ε″ verifies that the nanocomposite samples exhibit dielectric behavior, making them potential nanodielectric materials for usage in biomaterials, capacitors, and antennas within the microelectronic sector. Systematic variations in Er_2O_3 nanoparticle concentration within the PVA matrix were studied to understand the correlation between nanoparticle content and dielectric properties. The dielectric constant showed a concentration-dependent trend, indicating that the presence of Er_2O_3 nanoparticles plays a crucial role in shaping the dielectric response of the composite. This information is vital for tailoring the dielectric properties according to specific application requirements.

Frequency-dependent dielectric studies were conducted to examine the material's response over a broad frequency spectrum. The PEr films exhibited stable dielectric properties, with a relatively constant dielectric constant across the studied frequencies. This stable behavior indicates the material's suitability for applications where consistent dielectric performance is essential, such as in electronic devices operating at various frequency ranges. The observed structural changes, including crystallinity and morphology, directly impact the electrical and dielectric performance. Enhanced conductivity is attributed to the improved intermolecular interactions facilitated by the presence of Er_2O_3, while the dielectric properties benefit from the increased polarizability.

3.4. Conductivity characterization of PEr films

For the polymeric samples, the AC conductivity values at room temperature are displayed in Fig. 10. Conductivity measurements of PEr films reveal a substantial enhancement compared to pristine PVA films when exposed to external electrical fields and Er_2O_3 content [66]. The incorporation of Er_2O_3 nanoparticles within the PVA matrix facilitates charge transport, resulting in improved electrical conductivity. The conductivity in nanocomposite samples can be affected by the interfaces between the electrodes and electrolytes at lower frequency ranges. With a lower frequency, ions may remain for a longer time, which results in more accumulation of charges at the interfaces between the electrodes and electrolytes [67]. Since the charge carrier is unable to move as quickly as it should, the conductivity drops. The electrical conductivity is scattered at higher frequencies; this dispersion is associated with rapid ion back-hopping and can be characterized by the bulk relaxation

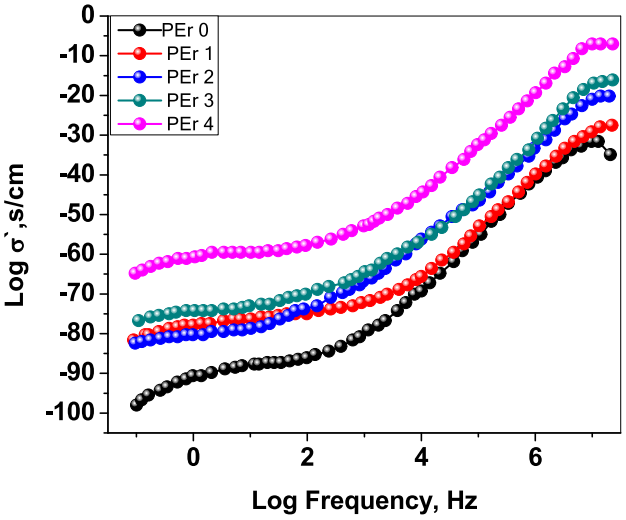

Fig. 10. Variation conductivity of PEr nanocomposite films.

phenomena. Adding Er_2O_3 nanoparticles to a PVA film may increase the number of mobile charge carriers, which in turn increases the AC conductivity. Interactions and intermolecular hydrogen bonding within the polymeric structure will boost ionic conductivity. This was demonstrated by the complex interaction between the PVA film and the Er_2O_3 nanoparticles.

The observed conductivity characteristics offer insights into the charge transport mechanisms within the PEr films. Whether dominated by tunneling, hopping, or percolation, understanding the underlying mechanisms is crucial for tailoring the material for specific conductivity requirements in diverse applications. The observed conductivity behavior with varying Er_2O_3 concentration provides insights into the percolation threshold, where a critical nanoparticle concentration is reached, leading to the formation of a conductive network throughout the composite. Understanding this threshold is crucial for designing materials with specific conductivity requirements. This is why the AC conductivity improved after Er_2O_3 nanoparticles were added, as the Er_2O_3 nanoparticles ' content increased [68,69]. The enhanced conductivity of PVA- Er_2O_3 films positions them as promising candidates for various electronic devices, sensors, and energy storage systems. The enhanced dielectric constant and low dielectric loss exhibited by the PEr films make them ideal candidates for sensor applications, particularly in capacitive and resistive sensors. The addition of Er_2O_3 nanoparticles

improves the material's sensitivity to external stimuli (e.g., temperature, pressure, or electric fields) due to their polar nature and the material's ability to exhibit strong polarization behavior. This allows for better signal detection and response in sensor systems. Moreover, the tunability of the dielectric properties by varying the Er_2O_3 concentration enables the optimization of these films for specific sensing environments. The high dielectric constant of PEr films enhances their charge storage capability, which is essential for capacitors and energy storage systems. The ability of these films to store electrical energy efficiently, along with their good thermal stability and mechanical properties, makes them suitable for applications in supercapacitors and dielectric capacitors. The dielectric loss, which remains low, ensures minimal energy dissipation during charge and discharge cycles, thus improving the overall efficiency and lifespan of energy storage devices.

3.4.1. Argand plot characterization of PEr films

The dielectric behavior of PEr films was analyzed through Argand plots, constructed from impedance spectroscopy data. Argand plot is used to analyze the complex impedance data of the PVA-Er_2O_3 films. The impedance Z can be expressed as a complex number, where $Z = M'+jM''$. The real part M' and the imaginary part M'' of the impedance are given by the following equations [57]:

$$M' = \varepsilon'/(\varepsilon'^2 + \varepsilon''^2) \quad (9)$$

$$M'' = \varepsilon''/(\varepsilon'^2 + \varepsilon''^2) \quad (10)$$

These plots, illustrating the real and imaginary parts of the impedance in the complex plane, provide insights into the material's electrical response. At room temperature, the electrolyte samples are displayed in Fig. 11 as M' vs M'' plots, also known as Argand plots.

The semi-circular shape of the Argand plot is indicative of a single relaxation process dominating the material's dielectric behavior. Deviations from this ideal shape may suggest the presence of multiple relaxation mechanisms or non-ideal behavior. The radius of the semi-circle corresponds to the magnitude of the impedance at the characteristic relaxation frequency. Changes in the radius can provide information about variations in the relaxation time of charge carriers within the material. The center of the semi-circle on the real axis corresponds to the real part of the impedance at the characteristic relaxation frequency. Shifts in the center reveal alterations in the conductivity or resistance of the material. Systematic variations in Er_2O_3 nanoparticle concentration within the PVA matrix were reflected in the Argand plots. Changes in the shape, size, or position of the semi-circle provide information about how nanoparticle concentration influences the dielectric properties. The Argand plot parameters were correlated with conductivity measurements to understand the relationship between the dielectric and electrical characteristics of PEr films. This correlation aids in deciphering the charge transport mechanisms and their manifestation in the impedance data. The unique dielectric characteristics revealed through Argand plot analysis position PEr films as promising candidates for integration into electronic devices.

3.5. Mechanical characteristics

The stress–strain curves of the polymer nanocomposite films comprising Er_2O_3 NPs are illustrated in Fig. 12, and the mechanical properties such as Young's modulus, tensile strength, stiffness, and elongation at fracture are provided in Table 3. When the number of nanoparticles in nanocomposite samples increases, the elongation at break becomes lower and other factors improve. It appears that the presence of Er_2O_3 nanoparticles enhances the samples' resistance to tensile stress and the strength of the polymeric chains in the obtained samples also improves. The nanocomposite sample, which contains 10 wt of nanocomposites, performs the pure PVA in terms of tensile strength and Young's modulus. The structure limits the mobility of PVA chains under tensile strain, which improves mechanical characteristics due to the suitable dispersion of included Er_2O_3 nanoparticles and their highly effective interfacial adhesion. Further, as the local density within the nanocomposite samples increases, both the stiffness and the elongation ratio at fracture values considerably rise [63].

4. Conclusion

In conclusion, this study has presented a comprehensive exploration of polyvinyl alcohol (PVA) films infused with Erbium Oxide (Er_2O_3) nanoparticles, aiming to enhance their optical, conductivity, and dielectric properties. The results and discussions provide key insights into the structural, optical, electrical, and dielectric attributes of the composite material. The structural analysis, through XRD and Raman spectra, confirmed the successful integration of Er_2O_3 nanoparticles within the PVA matrix, influencing the crystalline structure and surface morphology of the films. Insertion of Er_2O_3 into the PVA matrix declines the film's transparency and bandgap while raising its refractive index. The electrical conductivity measurements demonstrated a remarkable enhancement, showcasing the potential of PVA-Er_2O_3 films for applications demanding improved electrical performance. Systematic variations in Er_2O_3 concentration and film thickness revealed optimal conditions for maximizing conductivity, while temperature-dependent

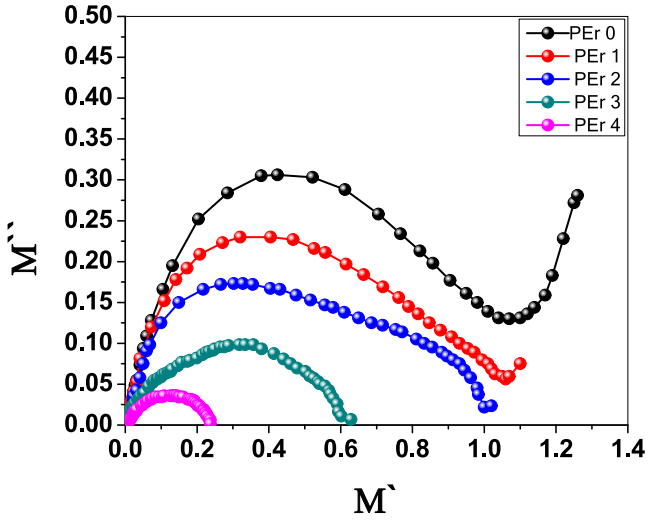

Fig. 11. The Argand graph of PEr nanocomposite films.

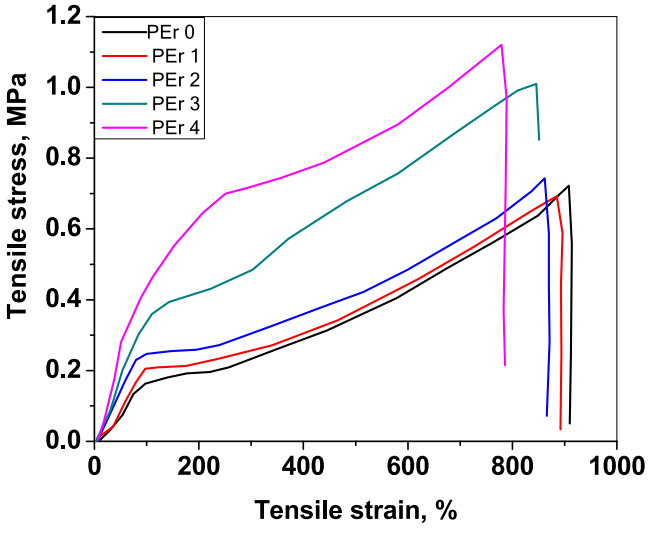

Fig. 12. Mechanical profile of PEr nanocomposite films.

Table 3
Mechanical characteristics of the PEr nanocomposite films.

Samples	Tensile Strength (MPa)	Young's Modulus (MPa)	Elongation at Fracture (%)
PEr0	0.65	305.12	925.12
PEr1	0.82	347.73	892.30
PEr2	0.96	724.65	871.32
PEr3	1.11	891.81	802.12
PEr4	1.23	951.07	754.37

studies provided insights into the thermal behavior of the material. The obtained results highlighted the material's stability and suitability for applications requiring consistent dielectric performance across different frequencies. The Argand plot analysis added another layer of sophistication to the study, providing a nuanced understanding of the charge transport mechanisms and dielectric relaxation behavior within PVA-Er_2O_3 films. The mechanical characteristics of the PVA-Er_2O_3 films were significantly enhanced. The stress–strain curves indicated that increasing the concentration of Er_2O_3 nanoparticles led to improved tensile strength and Young's modulus, while elongation at break decreased. The 10 wt% Er_2O_3 nanocomposite performed comparably to pure PVA in terms of tensile strength and Young's modulus, demonstrating enhanced resistance to tensile stress and stronger polymeric chains due to effective nanoparticle dispersion and interfacial adhesion. The synthesis and characterization of PVA-Er_2O_3 films represent a significant step forward in the development of advanced materials with enhanced conductivity and dielectric performance, holding promise for applications in electronics, sensors, and energy storage systems.

Ethical Approval

This article does not contain any studies with animals performed by any of the authors.

CRediT authorship contribution statement

T.S. Soliman: Writing – review & editing, Writing – original draft, Supervision, Methodology, Investigation, Formal analysis, Data curation, Conceptualization. **A. Khalid:** Writing – original draft, Formal analysis, Data curation, Conceptualization. **M. Khalid Hossain:** Writing – review & editing, Visualization, Validation. **Sherief A. Al kiey:** Writing – review & editing, Writing – original draft, Supervision, Methodology, Investigation, Formal analysis, Data curation, Conceptualization.

Declaration of competing interest

The authors declare that they have no known competing financial interests or personal relationships that could have appeared to influence the work reported in this paper.

Data availability

No data was used for the research described in the article.

References

[1] V. Vatanpour, O.O. Teber, M. Mehrabi, I. Koyuncu, Polyvinyl alcohol-based separation membranes: a comprehensive review on fabrication techniques, applications and future prospective, Mater. Today Chem. 28 (2023) 101381, https://doi.org/10.1016/j.mtchem.2023.101381.

[2] T.S. Gaaz, A.B. Sulong, M.N. Akhtar, A.A.H. Kadhum, A.B. Mohamad, A.A. Al-Amiery, D.J. McPhee, Properties and applications of polyvinyl alcohol, halloysite nanotubes and their nanocomposites, Molecules. 20 (2015) 22833–22847, https://doi.org/10.3390/molecules201219884.

[3] B.K. Tan, Y.C. Ching, S.C. Poh, L.C. Abdullah, S.N. Gan, A review of natural fiber reinforced poly(vinyl alcohol) based composites: Application and opportunity, Polymers (basel). 7 (2015) 2205–2222, https://doi.org/10.3390/polym7111509.

[4] M. Teodorescu, M. Bercea, S. Morariu, Biomaterials of Poly(vinyl alcohol) and Natural Polymers, Polym. Rev. 58 (2018) 247–287, https://doi.org/10.1080/15583724.2017.1403928.

[5] B. Karthikeyan, S. Hariharan, A. Sasidharan, V. Gayathri, T. Arun, A. Akbari-Fakhrabadi, C. Madhumitha, Optical, vibrational and fluorescence recombination pathway properties of nano SiO2-PVA composite films, Opt. Mater. (amst) 90 (2019) 139–144, https://doi.org/10.1016/J.OPTMAT.2019.01.063.

[6] O.G. Abdullah, S.B. Aziz, K.M. Omer, Y.M. Salih, Reducing the optical band gap of polyvinyl alcohol (PVA) based nanocomposite, J. Mater. Sci. Mater. Electron. 26 (2015) 5303–5309, https://doi.org/10.1007/s10854-015-3067-3.

[7] R. Ambrosio, A. Carrillo, M. Mota, K. de la Torre, R. Torrealba, M. Moreno, H. Vazquez, J. Flores, I. Vivaldo, Polymeric nanocomposites membranes with high permittivity based on PVA-ZnO nanoparticles for potential applications in flexible electronics, Polymers (basel). 10 (2018) 1370, https://doi.org/10.3390/polym10121370.

[8] S. Ningaraju, A.P. Gnana Prakash, H.B. Ravikumar, Studies on free volume controlled electrical properties of PVA/NiO and PVA/TiO2 polymer nanocomposites, Solid State Ionics. 320 (2018) 132–147, https://doi.org/10.1016/j.ssi.2018.03.006.

[9] V. Ghorbani, M. Ghanipour, D. Dorranian, Effect of TiO2/Au nanocomposite on the optical properties of PVA film, Opt. Quantum Electron. 48 (2016) 61, https://doi.org/10.1007/s11082-015-0335-7.

[10] B. Karthikeyan, S. Hariharan, R.V. Mangalaraja, T. Pandiyarajan, R. Udayabhaskar, P. Sreekanth, Studies on NiO-PVA composite films for opto-electronics and optical limiters, IEEE Photonics Technol. Lett. 30 (2018) 1539–1542, https://doi.org/10.1109/LPT.2018.2859042.

[11] M.A. Habeeb, A.H. Mohammed, Fabrication and tailored optical and electrical characteristics of Co2O3/SiC nanostructures doped PVA for multifunctional technological applications, Opt. Quantum Electron. 55 (2023) 1–17, https://doi.org/10.1007/s11082-023-05061-8.

[12] T.A. Hamdalla, T.A. Hanafy, A.E. Bekheet, Influence of erbium ions on the optical and structural properties of polyvinyl alcohol, J. Spectrosc. 2015 (2015), https://doi.org/10.1155/2015/204867.

[13] S.A.M. Issa, D.E. Abulyazied, A.W. Alrowaily, H.A. Saudi, E.S. Ali, A.M.A. Henaish, H.M.H. Zakaly, Improving the electrical, optical and radiation shielding properties of polyvinyl alcohol yttrium oxide composites, J. Rare Earths. (2023) 6–14, https://doi.org/10.1016/j.jre.2023.02.013.

[14] E. Kumi Barimah, S. Rahayu, M.W. Ziarko, N. Bamiedakis, I.H. White, R.V. Penty, G.M. Kale, G. Jose, Erbium-doped nanoparticle-polymer composite thin films for photonic applications: structural and optical properties, ACS Omega. 5 (2020) 9224–9232, https://doi.org/10.1021/acsomega.0c00040.

[15] G. Mohammed, S. El-Gamal, A.M. El Sayed, S. Saber, Synthesis, structural, optical and electrical characterization of Y2O3/poly(ethylene glycol)–poly(vinyl chloride) based nanocomposite solid polymer electrolytes, Polym. Int. 72 (2023) 342–355, https://doi.org/10.1002/PI.6472.

[16] S. Alhassan, K. Alshammari, M. Alshammari, T. Alotaibi, A.H. Alshammari, A. Alhamazani, M. Henini, T. Abdel Mohaymen Taha, Linear and nonlinear optical investigations of polyvinyl chloride modified La2O3 nanocomposite films, Results Phys. 58 (2024) 107456, https://doi.org/10.1016/j.rinp.2024.107456.

[17] M.Y.A. Mostafa, H.M.H. Zakaly, S.A.M. Issa, H.A. Saudia, A.M.A. Henaish, Tailoring variations in the linear optical and radiation shielding parameters of PVA polymeric composite films doped with rare-earth elements, Appl. Phys. A Mater. Sci. Process. 128 (2022) 199, https://doi.org/10.1007/s00339-022-05304-7.

[18] Y. Taşgin, M.E. Pekdemir, M. Yilmaz, M.S. Kanca, M. Kök, Physical and shielding properties of Er2O3 rare earth oxide compound content on PCL/PEG blend, Polym. Bull. 81 (2023) 2915–2931, https://doi.org/10.1007/s00289-023-04818-1.

[19] S. Chandra, J.B. Gruber, G.W. Burdick, D.K. Sardar, Fabrication and absorption intensity analyses of Er2O3 nanoparticles suspended in polymethyl methacrylate, J. Appl. Polym. Sci. 122 (2011) 289–295, https://doi.org/10.1002/app.

[20] A. El Askary, M. El-Sharnouby, N.S. Awwad, H.A. Ibrahium, M.A. El-Morsy, M. O. Farea, A.A. Menazea, Optical, thermal, and electrical conductivity strength of ternary CMC/PVA/Er2O3 NPs nanocomposite fabricated via pulsed laser ablation, Phys. B Condens. Matter. 637 (2022) 413910, https://doi.org/10.1016/j.physb.2022.413910.

[21] A.H. Alshammari, M. Alshammari, M. Ibrahim, K. Alshammari, T.A.M. Taha, New hybrid PVC/PVP polymer blend modified with Er2O3 nanoparticles for optoelectronic applications, Polymers (basel). 15 (2023) 684, https://doi.org/10.3390/polym15030684.

[22] A. Arya, M. Sadiq, A.L. Sharma, Effect of variation of different nanofillers on structural, electrical, dielectric, and transport properties of blend polymer nanocomposites, Ionics (kiel). 24 (2018) 2295–2319, https://doi.org/10.1007/s11581-017-2364-7.

[23] T.A. Taha, M.H. Mahmoud, Synthesis and characterization of PVDF-Er2O3 polymer nanocomposites for energy storage applications, Mater. Chem. Phys. 270 (2021) 124827, https://doi.org/10.1016/j.matchemphys.2021.124827.

[24] B. Kandasamy, S.B. Sussela, R. Sankararajan, Strontium-supported erbium oxide nanoparticles for efficient organic pollutant degradation under UV – Visible light, J. Mater. Sci. Mater. Electron. 33 (2022) 20384–20398, https://doi.org/10.1007/s10854-022-08855-w.

[25] A.I. Helal, S.A. Vshivkov, M.F. Zaki, S.I. Elkalashy, T.S. Soliman, Effect of carbon nano tube in the structural and physical properties of polyvinyl chloride films, Phys. Scr. 96 (2021) 085804, https://doi.org/10.1088/1402-4896/ABF86C.

[26] T.S. Soliman, M.M. Hessien, E. Sheha, Probing a new halogen-free electrolyte and Ba0.85Sm0.1TiO3 cathode for Mg battery applications, J. Mater. Sci. Mater. Electron. 32 (2021) 28781–28791, https://doi.org/10.1007/s10854-021-07263-w.

[27] K.S. Hemalatha, K. Rukmani, Synthesis, characterization and optical properties of polyvinyl alcohol-cerium oxide nanocomposite films, RSC Adv. 6 (2016) 74354–74366, https://doi.org/10.1039/c6ra11126b.
[28] A.A. Mohammed, M.A. Habeeb, Modification and development of the structural, optical and antibacterial characteristics of PMMA/Si3N4/TaC nanostructures, Silicon. 15 (2023) 5163–5174, https://doi.org/10.1007/s12633-023-02426-2.
[29] A. Hashim, A.J. Kadham Algidsawi, H. Ahmed, A. Hadi, M.A. Habeeb, Synthesis of PVA/PVP/SnO2 nanocomposites: Structural, optical, and dielectric characteristics for pressure sensors, Nanosistemi, Nanomater, Nanotehnologii. 19 (2021) 353–362.
[30] A. Hashim, H. Ahmed, A. Yahya, A. Hadi, M.A. Habeeb, Biopolymers–Metal Oxide Nanocomposites as Coating Materials for Biomedical Applications, Nanosistemi, Nanomater. Nanotehnologii. 19 (2021) 681–688. 10.15407/nnn.19.03.681.
[31] N.K. Al-Sharifi, M.A. Habeeb, Improvement structural and dielectric properties of PS/SiC/Sb2O3 nanostructures for nanoelectronics devices, East Eur. J. Phys. 2023 (2023) 341–347, https://doi.org/10.26565/2312-4334-2023-2-40.
[32] R.S.A. Hamza, M.A. Habeeb, Synthesis and tuning the structural, morphological and dielectric characteristics of PVA-CMC-SiO2–Cr2O3 hybrid nanostructures for nanoelectronics devices, Opt. Quantum Electron. 55 (2023) 1–18, https://doi.org/10.1007/s11082-023-04995-3.
[33] S.M. Mahdi, M.A. Habeeb, Low-cost piezoelectric sensors and gamma ray attenuation fabricated from novel polymeric nanocomposites, AIMS Mater. Sci. 10 (2023) 288–300, https://doi.org/10.3934/MATERSCI.2023015.
[34] M.A. Habeeb, W.H. Rahdi, Titanium carbide nanoparticles filled PVA-PAAm nanocomposites: structural and electrical characteristics for application in energy storage, Opt. Quantum Electron. 55 (2023) 1–18, https://doi.org/10.1007/s11082-023-04639-6.
[35] B. Li, J. Cao, X. Cao, B. Guo, H. Lu, Preparation and characterization of chemically crosslinked polyvinyl alcohol/carboxylated nanocrystalline cellulose nanocomposite hydrogel films with high mechanical strength, J. Macromol. Sci. Part B Phys. 55 (2016) 518–531, https://doi.org/10.1080/00222348.2016.1171068.
[36] S.A. Paralikar, J. Simonsen, J. Lombardi, Poly(vinyl alcohol)/cellulose nanocrystal barrier membranes, J. Memb. Sci. 320 (2008) 248–258, https://doi.org/10.1016/j.memsci.2008.04.009.
[37] R. Sabarish, G. Unnikrishnan, Polyvinyl alcohol/carboxymethyl cellulose/ZSM-5 zeolite biocomposite membranes for dye adsorption applications, Carbohydr. Polym. 199 (2018) 129–140, https://doi.org/10.1016/j.carbpol.2018.06.123.
[38] A.M. El-Hadi, Increase the elongation at break of poly (lactic acid) composites for use in food packaging films, Sci. Rep. 7 (2017) 1–14, https://doi.org/10.1038/srep46767.
[39] Y. Li, T. Yang, T. Yu, L. Zheng, K. Liao, Synergistic effect of hybrid carbon nantube-graphene oxide as a nanofiller in enhancing the mechanical properties of PVA composites, J. Mater. Chem. 21 (2011) 10844–10851, https://doi.org/10.1039/c1jm11359c.
[40] M.R. Joya, J.E. Alfonso, L.C. Moreno, Photoluminescence and Raman studies of α -MoO3 doped with erbium and neodymium, Curr. Sci. 116 (2019) 1690–1695, https://doi.org/10.18520/cs/v116/i10/1690-1695.
[41] J. Castaneda-Contreras, V.F. Maranon-Ruiz, M.A. Meneses-Nava, H.-P.-L. de Guevara, R.A.R. Rojas, R. Chiu-Zarate, Properties of Er2O3 nanoparticles synthesized by a modified co-precipitation method, Rev. Mex. Física. 61 (2015) 127–131.
[42] C.C. Yang, Y.J. Lee, S.J. Chiu, K.T. Lee, W.C. Chien, C.T. Lin, C.A. Huang, Preparation of a PVA/HAP composite polymer membrane for a direct ethanol fuel cell (DEFC), J. Appl. Electrochem. 38 (2008) 1329–1337, https://doi.org/10.1007/s10800-008-9563-x.
[43] K. SK, V. N, B. RB, S. Madivalappa, Structural and optical properties of polyvinyl alcohol/copper oxide (PVA/CuO) nanocomposites, Solid State Commun. 370 (2023) 115221. 10.1016/j.ssc.2023.115221.
[44] B. Priya, V.K. Gupta, D. Pathania, A.S. Singha, Synthesis, characterization and antibacterial activity of biodegradable starch/PVA composite films reinforced with cellulosic fibre, Carbohydr. Polym. 109 (2014) 171–179, https://doi.org/10.1016/j.carbpol.2014.03.044.
[45] A.K. Nikolaidis, D.S. Achilias, Thermal degradation kinetics and viscoelastic behavior of poly(methyl methacrylate)/ organomodified montmorillonite nanocomposites prepared via in situ bulk radical polymerization, Polymers (basel). 10 (2018), https://doi.org/10.3390/polym10050491.
[46] Q.A. Alsulami, A. Rajeh, Modification and development in the microstructure of PVA/CMC-GO/Fe3O4 nanocomposites films as an application in energy storage devices and magnetic electronics industry, Ceram. Int. 49 (2023) 14399–14407, https://doi.org/10.1016/j.ceramint.2023.01.029.
[47] T.S. Soliman, S.I. Elkalashy, M.F. Zaki, D.H. Shabaan, Structural and optical analysis of gamma-induced modification in polycarbonate nuclear track detector, Phys. Scr. 96 (2021) 125814.
[48] M.F. Zaki, S.I. Elkalashy, T.S. Soliman, A comparative study of the structural, optical and morphological properties of different types of Makrofol polycarbonate, Polym. Bull. 79 (2022) 10841–10863, https://doi.org/10.1007/s00289-021-04011-2.
[49] S. Madivalappa, R.B. Basavaraj, P.B. Chethan, D.P. Aarti, P.K. Jisha, Insights and perspectives on PVDF/MgO NCs films: structural and optical properties for optoelectronic device applications, Results Chem. 11 (2024) 101764, https://doi.org/10.1016/j.rechem.2024.101764.
[50] A. Hashim, M.H. Abbas, N.A.H. Al-Aaraji, A. Hadi, Facile fabrication and developing the structural, optical and electrical properties of SiC/Y2O3 nanostructures doped PMMA for optics and potential nanodevices, Silicon. 15 (2023) 1283–1290, https://doi.org/10.1007/s12633-022-02104-9.
[51] M.N. Azlan, M.K. Halimah, S.Z. Shafinas, W.M. Daud, Polarizability and optical basicity of Er3+ ions doped tellurite based glasses, Chalcogenide Lett. 11 (2014) 319–335.
[52] A. Badawi, S.S. Alharthi, The optical, electrical and mechanical performance of metal oxides incorporated PVA/rGO blend: effect of metal oxide type, Appl. Phys. A Mater. Sci. Process. 128 (2022) 1–15, https://doi.org/10.1007/S00339-022-05495-Z/FIGURES/11.
[53] V. Dimitrov, S. Sakka, Linear and nonlinear optical properties of simple oxides. II, J. Appl. Phys. 79 (1996) 1741–1745, https://doi.org/10.1063/1.360963.
[54] S.A. Umar, M.K. Halimah, K.T. Chan, A.A. Latif, Polarizability, optical basicity and electric susceptibility of Er3 + doped silicate borotellurite glasses, J. Non. Cryst. Solids. 471 (2017) 101–109, https://doi.org/10.1016/j.jnoncrysol.2017.05.018.
[55] S.A. Al Kiey, S.A.M. Abdel-Hameed, M.A. Marzouk, Influence of transition metals on the development of semiconducting and low thermal expansion TiO2-borosilicate glasses and glass ceramics, Silicon. (2024), https://doi.org/10.1007/s12633-024-02896-y.
[56] A. Darwish, N.S. El-Sayed, S.A. Al Kiey, S. Kamel, G. Turky, Polyanionic electrically conductive superabsorbent hydrogel based on sodium alginate-g-poly (AM-co-ECA-co-AMPS): broadband dielectric spectroscopy investigations, Int. J. Biol. Macromol. 232 (2023) 123443, https://doi.org/10.1016/j.ijbiomac.2023.123443.
[57] A.M. Fahim, R.E. Abouzeid, S.A.A. Kiey, S. Dacrory, Development of semiconductive foams based on cellulose- benzenesulfonate/CuFe2O4-nanoparticles and theoretical studies with DFT/ B3PW91/LANDZ2 basis set, J. Mol. Struct. 1247 (2022) 131390, https://doi.org/10.1016/j.molstruc.2021.131390.
[58] S.A. Al Kiey, M. Toderaş, O.A. Al-Qabandi, M. Bassyouni, Q. Zhou, M. El Fray, M. S. Hasanin, Investigating the hybrid potential of PVA-chitosan-loaded TiO2@NiO films for advanced conductivity and dielectric performance, Polym. Test. 138 (2024) 108546, https://doi.org/10.1016/j.polymertesting.2024.108546.
[59] S.A. Al Kiey, A.A. Menazea, A.M. Ismail, Flexible free standing electrodes based on laser-irradiated PVC/PVDF/AuNPs for the development of high performance supercapacitor electrodes, J Energy Storage. 72 (2023) 108723, https://doi.org/10.1016/j.est.2023.108723.
[60] N.S. El-Sayed, S.A. Al Kiey, A. Darwish, G. Turky, S. Kamel, High performance hydrogel electrodes based on sodium alginate-g-poly(AM-c o-ECA-co-AMPS for supercapacitor application, Int. J. Biol. Macromol. 218 (2022) 420–430, https://doi.org/10.1016/j.ijbiomac.2022.07.117.
[61] H.M. Ragab, Enhancement in optical, thermal and electrical properties of Polyvinyl pyrrolidone/ polyethylene oxide matrix-based nanocomposites for advanced flexible optoelectronic technologies considering nanoceramic zinc oxide/titanium dioxide filler, J. Mol. Struct. 1275 (2023) 134663, https://doi.org/10.1016/j.molstruc.2022.134663.
[62] E.M. Abdelrazek, I.S. Elashmawi, A.M. Hezma, A. Rajeh, M. Kamal, Effect of an encapsulate carbon nanotubes (CNTs) on structural and electrical properties of PU/PVC nanocomposites, Phys. B Condens. Matter. 502 (2016) 48–55, https://doi.org/10.1016/j.physb.2016.08.040.
[63] S. Demirezen, S.A. Yerişkin, Frequency and voltage-dependent dielectric spectroscopy characterization of Al/(Coumarin-PVA)/p-Si structures, J. Mater. Sci. Mater. Electron. 32 (2021) 25339–25349, https://doi.org/10.1007/s10854-021-06993-1.
[64] E. Salim, A.E. Tarabiah, The influence of NiO nanoparticles on structural, optical and dielectric properties of CMC/PVA/PEDOT:PSS nanocomposites, J. Inorg. Organomet. Polym. Mater. 33 (2023) 1638–1645, https://doi.org/10.1007/s10904-023-02591-2.
[65] A.A. Al-Muntaser, R.A. Pashameah, A. Saeed, R. Alwafi, E. Alzahrani, S.A. AlSubhi, A.Y. Yassin, Boosting the optical, structural, electrical, and dielectric properties of polystyrene using a hybrid GNP/Cu nanofiller: novel nanocomposites for energy storage applications, J. Mater. Sci. Mater. Electron. 34 (2023) 1–14, https://doi.org/10.1007/s10854-023-10104-7.
[66] M.R. Atta, N. Algethami, M.O. Farea, Q.A. Alsulami, A. Rajeh, Enhancing the structural, thermal, and dielectric properties of the polymer nanocomposites based on polymer blend and barium titanate nanoparticles for application in energy storage, Int. J. Energy Res. 46 (2022) 8020–8029, https://doi.org/10.1002/er.7703.
[67] C. Yan, R. Xu, Y. Xiao, J.F. Ding, L. Xu, B.Q. Li, J.Q. Huang, Toward critical electrode/electrolyte interfaces in rechargeable batteries, Adv. Funct. Mater. 30 (2020) 1–21, https://doi.org/10.1002/adfm.201909887.
[68] A.N. Al-Hakimi, G.M. Asnag, F. Alminderej, I.A. Alhagri, S.M. Al-Hazmy, T. F. Qahtan, Enhancing the structural, optical, thermal, and electrical properties of PVA filled with mixed nanoparticles (TiO2/Cu), Crystals. 13 (2023), https://doi.org/10.3390/cryst13010135.
[69] N. Algethami, A. Rajeh, H.M. Ragab, A.E. Tarabiah, F. Gami, Characterization, optical, and electrical properties of chitosan/polyacrylamide blend doped silver nanoparticles, J. Mater. Sci. Mater. Electron. 33 (2022) 10645–10656, https://doi.org/10.1007/s10854-022-08048-5.

Dr. T. S. Soliman is an Associate Professor of Solid-State Science at Benha University, Egypt. He currently, works as a researcher at Ural Federal University, Ekaterinburg, Russia. Dr. T. S. Soliman is an academic editor in the journal "*Advances in Polymer Technology*" at Wiley. He is concerned with the fabrication of polymer and polymer blend nanocomposite materials, and the investigation of their physical properties, besides the influence of gamma rays on polymer materials' structural and physicochemical properties. He obtained his Ph.D. in polymer science in 2016 from Ural Federal University, Russia. According to SCOPUS, he has published around 44 papers in his field. He also reviewed many articles from reputable journals in his field.

Dr. A. Khalid is a lecturer in material science and optical material at Department of Basic Engineering Sciences, Faculty of Engineering at Shoubra, Benha University, Cairo, Egypt. He focuses on synthesis of nanomaterials, polymer nanocomposites, and their optical and thermal properties characterization. He is also interested in renewable energy, including the third generation of solar cells.

Dr. M. Khalid Hossain has been classified as the world's Top 2% most-cited researcher in "Energy", & "Applied Physics", (Aug 2024); and in "Nanoscience & Nanotechnology" (Oct 2023), published by Stanford University & Elsevier. Dr. Hossain has been working in the area of nanostructured materials, chemistry and physics of ceramics materials, and thin-film technology for over 15 years. He obtained his Ph.D. for the fundamental study of rare-earth oxides and perovskite proton conducting oxides in 2021 from Kyushu University, Japan. He is currently affiliated as a Senior Research Scientist in the Bangladesh Atomic Energy Commission. His recent research work focuses on the application of nanostructured materials in the energy field, nanoparticles, ceramics and composites, and the characterization of materials. Dr. Hossain has published more than 250 research papers in peer-reviewed SCI(E) journals, books, and technical conference proceedings relevant to materials science and engineering. He also reviewed a significant number of articles from reputed journals in his discipline. Dr. Hossain is a Member of the American Ceramic Society, a Life Member of the Bangladesh Physical Society, and Bangladesh Electronic Society among others. He is also a member of the Bangladesh Atomic Energy Scientist Association.

Dr. Sherief A. Alkiey is a researcher in corrosion and electrochemistry at the Physical Chemistry department, National Research Centre, Cairo, Egypt. His expertise extends to TGA technique, Li-ion batteries, nanoparticle characterization, and polymer analysis. He has published around 45 papers in his field.